Published in final edited form as:
Biomacromolecules. 2013 March 11; 14(3): 900–909. doi:10.1021/bm301995s.

Two-Dimensional Nanostructure- Reinforced Biodegradable Polymeric Nanocomposites for Bone Tissue Engineering

Gaurav Lalwani[1], **Allan M. Henslee**[2], **Behzad Farshid**[3], **Liangjun Lin**[1], **F. Kurtis Kasper**[2], **Yi-Xian Qin**[1], **Antonios G. Mikos**[2], and **Balaji Sitharaman**[1,*]

[1]Department of Biomedical Engineering, Stony Brook University, Stony Brook, NY 11794-5281, USA

[2]Department of Bioengineering, Rice University, Houston, Texas 77251-1892, USA

[3]Department of Materials Science and Engineering, Stony Brook University, Stony Brook, NY 11794, USA

Abstract

This study investigates the efficacy of two dimensional (2D) carbon and inorganic nanostructures as reinforcing agents of crosslinked composites of the biodegradable and biocompatible polymer polypropylene fumarate (PPF) as a function of nanostructure concentration. PPF composites were reinforced using various 2D nanostructures: single- and multi-walled graphene oxide nanoribbons (SWGONRs, MWGONRs), graphene oxide nanoplatelets (GONPs), and molybdenum di-sulfite nanoplatelets (MSNPs) at 0.01–0.2 weight% concentrations. Cross-linked PPF was used as the baseline control, and PPF composites reinforced with single- or multi-walled carbon nanotubes (SWCNT, MWCNT) were used as positive controls. Compression and flexural testing show a significant enhancement (i.e., compressive modulus = 35–108%, compressive yield strength = 26–93%, flexural modulus = 15–53%, and flexural yield strength = 101–262% greater than the baseline control) in the mechanical properties of the 2D-reinforced PPF nanocomposites. MSNPs nanocomposites consistently showed the highest values among the experimental or control groups in all the mechanical measurements. In general, the inorganic nanoparticle MSNPs showed a better or equivalent mechanical reinforcement compared to carbon nanomaterials, and 2-D nanostructures (GONP, MSNP) are better reinforcing agents compared to 1-D nanostructures (e.g. SWCNTs). The results also indicate that the extent of mechanical reinforcement is closely dependent on the nanostructure morphology and follows the trend nanoplatelets > nanoribbons > nanotubes. Transmission electron microscopy of the cross-linked nanocomposites indicates good dispersion of nanomaterials in the polymer matrix without the use of a surfactant. The sol-fraction analysis showed significant changes in the polymer cross-linking in the presence of MSNP (0.01–0.2 wt %) and higher loading concentrations of GONP and MWGONR (0.1–0.2 wt%). The analysis of surface area and aspect ratio of the nanostructures taken together with the above results indicates differences in nanostructure architecture (2D vs. 1D nanostructures), as well as the chemical compositions (inorganic vs. carbon nanostructures), number of functional groups, and structural defects for the 2D nanostructures maybe key properties that affect the mechanical properties of 2D nanostructure-reinforced PPF nanocomposites, and the reason for the enhanced mechanical properties compared to the controls.

[*]Correspondence: Balaji Sitharaman, Ph.D., Department of Biomedical Engineering, Bioengineering Building Room 115, Stony Brook University, Stony Brook, NY 11794-5281, Tel: 631-632-1810, balaji.sitharaman@stonybrook.edu.

Introduction

The limitations in the clinical treatment of bone defects using autologous or allogenous bone grafts, and permanent prosthetic implants has led to emergence of bone tissue engineering strategies.[1] There has especially been a growing interest to develop nanoparticle-reinforced biodegradable polymer nanocomposites for bone tissue engineering applications.[2–6] A major motivation behind these studies is to enhance the mechanical properties of the biodegradable polymer for improved structural integrity when implanted under load bearing conditions. Carbon nanostructures such as the zero-dimensional fullerenes and one-dimensional single-walled carbon nanotubes (SWCNTs) have been extensively investigated as reinforcing agents in these studies.[2, 3, 5]

Recently, the unique physiochemical properties of two-dimensional carbon and inorganic nanostructures such as graphene oxide nanoplatelets,[7] graphene oxide nanoribbons,[8] and molybdenum disulfide nanoplatelets[9, 10] have been harnessed for a variety of potential applications such as water filtration membranes,[11] enabling components in energy and semiconductor electronic devices,[10, 12] dispersing agents for processing of solids liquid crystals,[13] solid lubricants,[9] porous scaffolds for tissue engineering,[14, 15] and agents for bioimaging and drug delivery.[13, 16, 17] Theoretical and experimental studies also show that 2D inorganic (e.g. molybdenum di-sulfite nanoparticles) and carbon (e.g. graphene nanoparticles) nanostructures also show remarkable mechanical properties.[18–20] For instance, graphene has been predicted to have remarkable mechanical stiffness comparable to graphite, and fracture strength similar to SWCNTs.[7, 21] Thus, for a 2D nanostructure-reinforced polymer nanocomposite under mechanical stress, the 2D nanostructure possessing high stiffness should allow efficient transfer of load from the polymer matrix.[22] Moreover, the 2D nanostructures show high surface area, structural defects, and the presence of functional groups (hydroxyl, carboxyl or sulfide groups) that should allow the formation of good interfaces with the polymer matrix; key requirements for efficient load transfer.[22] Thus, due to these potential benefits, the efficacy of 2D nanostructures as fillers to improve the mechanical properties of polymeric composites needs to be systematically investigated.

In this study, polymer poly(propylene fumarate) (PPF), an injectable, cross-linkable, and biodegradable polymer widely investigated for applications in bone tissue engineering was used as the polymer matrix.[2–5, 23–25] PPF nanocomposites were fabricated by dispersing 2D carbon (graphene oxide nanoplatelets (GONPs), single wall graphene oxide nanoribbons (SWGONRs), multi wall graphene oxide nanoribbons (MWGONRs)), or inorganic (MoS_2 nanoplatelets (MSNPs)) nanostructures as fillers into PPF at loading concentrations between 0.01–0.2 weight%. The characterization of structural, mechanical and crosslinking density of the nanocomposites were performed to investigate the effects of 2D nanostructure size, morphology, and chemical composition on their mechanical (compressional and flexural) properties.

Materials and Methods

Materials

Hydroquinone, *N*-vinyl-pyrrolidone (NVP), zinc chloride, potassium permanganate and benzoyl peroxide (BP) were purchased from Sigma Aldrich (New York, USA). Propylene glycol, ethyl ether, methylene chloride, sodium sulfate, hydrogen peroxide and chloroform (HPLC grade) were purchased from Fisher Scientific (Pittsburgh, PA, USA). Diethyl fumarate was purchased from Acros Organics (Fair Lawn, NJ, USA)

Single walled carbon nanotubes (SWCNTs, Cat. No. 698695), multiwalled carbon nanotubes (MWCNTs, Cat. No. 636487), graphite flakes (Cat. No. 496596), molybdenum

tri-oxide (Cat. No. M0753) and sulfur (Cat. No. 414980) were purchased from Sigma Aldrich (New York, USA). Organic solvents were reagent grade and used as received.

Synthesis of Polypropylene Fumarate

PPF was synthesized using a two-step reaction of diethyl fumarate and propylene glycol as described previously, and characterized by ^{1}H-NMR, and gel permeation chromatography.[26] Molecular weight distribution was measured by GPC system with a differential RI detector using a Styragel HR2 column (7.8 × 300 mm, Waters, MA). Chloroform at 1ml/min flow rate was used as the mobile phase. A calibration curve using polystyrene standards (Fluka, Switzerland) was used to determine PPF molecular weights. PPF batches of Mn = 3138 (PDI = 1.38) and Mn = 3808 (PDI = 1.44) were used for compression and three-point bending tests, respectively.

Synthesis of nanomaterials

Single- and multi-walled graphene oxide nanoribbons were synthesized from SWCNTs and MWCNTs via longitudinal unzipping method.[8] Graphene oxide nanoplatelets were synthesized using a modified Hummers method[27] and nano-hexagonal molybdenum di-sulfite nanoplatelets were synthesized using previously reported method.[28]

Raman spectroscopy

Raman spectroscopy was performed using a WITec alpha300R Micro-Imaging Raman Spectrometer using a 532 nm Nd-YAG excitation laser. Point spectra were recorded between 50–3750 cm^{-1} at room temperature.

Atomic Force Microscopy

Nanomaterials were dispersed in 1:1 ethanol:water by probe sonication (Cole-Parmer Ultrasonicator LPX 750) for one minute using 1 sec ‘on’ and 2 sec ‘off’ cycle. 50μl of homogenously dispersed nanomaterial solution was spin coated on freshly cleaved silicon wafers (Ted Pella, USA) at 3000 rpm for 5 minutes and used for AFM Imaging. AFM images were obtained using a NanoSurf EasyScan 2 Flex AFM (NanoScience Instruments Inc, Phoenix), operating in tapping mode, using a V-shaped cantilever (APP Nano ACL – 10, frequency f_c = 145–230 kHz, L = 225 μm, W = 40 μm, tip radius < 10 nm, spring constant k = 20–95 N/m). All images were collected under ambient conditions at 50% relative humidity and 25°C.

Surface Area Analysis

The surface area of nanostructures were measured using ABET series Brunauer-Emmett-Teller (BET) sorptometer at 77 K using nitrogen as the adsorption gas for SWCNT and MWCNT and krypton for SWGONR, MWGONR, GONP and MSNP at Porous Materials Inc., Ithaca, NY. Single point analysis was performed for all the samples.

Nanocomposite preparation

PPF and NVP were mixed in chloroform at a mass ratio of 1:1. Nanomaterials were dispersed in chloroform by bath sonication (Fisher Scientific) for 15 minutes followed by probe sonication (Cole Parmer, USA) for 1 minute using a 1 second ‘on’ and 2 second ‘off’ cycle and then added to the PPF-NVP mixture at concentrations of 0.1 to 2 wt%. The nanocomposite mixture was then sonicated for 15 minutes using a bath sonicator and chloroform was removed using a rotary evaporator (Büchi, Switzerland).

Thermal cross-linking and specimen fabrication

Thermal cross-linking of nanocomposite formulations was triggered by the addition of 1 wt % benzoyl peroxide (free radical initiator). BP was dissolved in diethyl fumarate at a concentration of 0.1 mg/ml and added to the nanocomposite mixture to initiate polymerization. The polymeric mixture was poured into prefabricated Teflon® (McMaster-Carr, Cleveland, OH) molds for compression testing (cylinders, 6.5 mm diameter and 14 mm length) and flexural testing (strips, 70 mm length, 12.7 mm width and 3.2 mm depth) and cured at 60°C for 24 hours. The specimens for compression and flexural testing were cut according to ASTM standards using a low-speed diamond saw (Model 650, South Bay Technology, San Clemente, CA, USA). Compression testing specimen dimensions were 6.5 mm diameter and 12 mm length. Flexural testing specimens were 65 mm long, 12.7 mm wide and 3.2 mm thick.

Mechanical Testing

Compressive and flexural mechanical testing were performed for n=5 samples using a Material Testing System mechanical testing machine (858 Mini Bionix II, MTS Systems, Eden Prairie, MN, USA) using a 5 kN load cell, at room temperature. American Society for Testing and Materials (ASTM) Standard D695-08 was followed for compression testing. Cylindrical specimens were compressed along their longitudinal axis until failure and force and displacement were recorded throughout the tests that were converted to stress and strain curves based on the initial sample dimensions. The slope of the initial linear portion of the stress-strain curve gave the compressive modulus. A line drawn parallel to the compressive modulus at 1.0% strain offset intersected the stress-strain curve giving the compressive yield strength.

Flexural testing was performed according to ASTM standard D790-07 using a three point bending apparatus. Samples were placed on two support spans 55 mm from each other and loaded midway until failure. Force and displacement values were recorded throughout the test. Flexural modulus was calculated using the following equation:

$$E_B = L^3 m / 4bd^3$$

Flexural Strength was calculated using the equation:

$$\sigma_{fM} = 3PL / 2bd^2$$

Where E_B = modulus of elasticity in bending (MPa), σ_{fM} = stress in the outer fibers at the midpoint (MPa), P = load at yield point at the load-deflection curve (N), L = support span (mm), b = width of the beam tested (mm), d = depth of the beam tested (mm) and, m = slope of the tangent to the initial straight line portion of the load – deflection curve (N/mm).

Sol Fraction Analysis

Sol fraction analysis was performed to assess the changes in the cross-linking density of the polymer in the presence of nanomaterials. Uncross-linked PPF, PPF/NVP and their oligomers are soluble in methylene chloride whereas cross-linked polymer is not. For assessment, a sample of approximately 0.1 g was weighed (W_i, accuracy 0.0001 g) and placed into a scintillation vial containing 20 ml methylene chloride. The vial was sealed and placed on the shaker (80 rpm) for 7 days. The remaining solid fraction was filtered with a weighed filter paper (W_p) and dried at room temperature for 1 hour followed by 60°C for an

additional 1 hour. The filter paper was weighed again (W_{p+s}) and the sol fraction was assessed for n=5 samples using the equation:

$$Sol\,fraction = \left(\frac{W_i - \left(W_{p+s} - W_p \right)}{W_i} \right) * 100$$

Transmission Electron Microscopy

TEM imaging for characterization of nanomaterials was carried out using JOEL 2100F high-resolution analytical transmission electron microscope (Centre for Functional Nanomaterials, Brookhaven National Laboratory, NY, USA) at an accelerating voltage of 200 kV. Samples were prepared by dispersing nanomaterials in 1:1 mixture of water/ethanol by probe sonication for 1 min using a 2 sec 'on', 1 sec 'off' cycle (Cole Parmer Ultrasonicator LPX 750) followed by ultracentrifugation at 5000 rpm for 5 minutes. The supernatant was dropped onto 300-mesh size, holey lacey carbon grids (Ted Pella, USA). Crosslinked nanocomposites were sectioned into 50–100 nm thick sections, mounted on copper mesh grids and imaged using a FEI BioTwinG^2 Transmission Electron Microscope at 80 kV.

Statistical Analysis

All statistical analysis were performed for n=5 samples using a 95% confidence interval. The data from mechanical testing and sol fraction analysis has been represented as mean ± standard deviation. One-way ANOVA followed by Tukey-Kramer post hoc analysis was used for comparisons between multiple groups.

Results and Discussions

SWGONR, MWGONR, GONP, MSNPs, and PPF were synthesized by well-established literature methods.[8, 26–28] The cross-linked nanoparticle-reinforced PPF nanocomposites and PPF composites were also fabricated using literature methods.[2, 5] Nanomaterial loading concentrations between 0.01–0.2 wt % were used to overcome several limitations associated with handling, processing, and fabrication of PPF nanocomposites for example, PPF nanocomposites possessing high nanomaterial loading (> 0.2 wt% SWCNTs) behave as viscoelastic solids.[3, 5, 24]

Figure 1 A displays the structural characterization of the 2D nanostructures by atomic force microscopy (AFM) and transmission electron microscopy (TEM). SWGONRs [Figures 1A (a) and (e)], and MWGONRs [Figures 1A (b) and (f)] are single- and multi- layered, respectively. Their nanoribbon structure appears uniform and smooth, with few edge defects. AFM images of SWGONRs [Figure 1A (a)] show that they possess an average width of 3–6 nm and length 500–1000 nm; confirming complete unzipping of SWCNT (diameter 1–2 nm, length 1–1.5 μm, width of nanoribbon = π * diameter). AFM height profile [inset, Figure 1A (a)] indicates that SWGONRs are single layered graphene oxide sheets (Z ≈ 1 nm). Due to the displacement of the sp^3 hybridized carbon, and the presence of oxygen, SWGONRs are expected to be slightly thicker than pristine graphene sheet which possesses a van der Waals thickness of 0.34 nm.[29, 30] MWGONRs have an average width of 60–90 nm corresponding to the complete unzipping of MWCNTs possessing diameter ranging from 20–30 nm (π * diameter). MWGONRs are 500 nm to 1500 nm long and have a height (Z) of about 7 nm (AFM height profile, inset Figure 1A (a)) corresponding to ≈ 21 graphene layers [value calculated assuming single layer graphene = 0.34 nm]. GONPs [Figure 1A (c) and (g)] are disk-shaped with ≈ 10–40 nm in diameter and 3–5 nm in height,

corresponding to ≈ 9–14 graphene layers. MSNPs [Figures 1A (d) and (h)] are hexagonal in shape, with diameter between 50–200 nm and height (Z) ≈ 8 nm.

The Raman spectra of SWGONRs, MWGONRs, GONPs and MSNPs are presented in Figure 1 B. The spectrum of pristine SWCNTs and MWCNTs has also been included for comparative purposes. Raman peaks were observed at 1343 cm^{-1} and 1596 cm^{-1} for SWGONRs, 1340 cm^{-1} and 1580 cm^{-1} for MWGONRs, and 1351 cm^{-1} and 1604 cm^{-1} for GONPs. Increase in the D band intensity was observed in the spectra of SWGONRs, MWGONRs and GONPs indicating increase in the disorder due to disruption of the sp^2 domains (pi-bonded C=C networks).[8, 31] Characteristic peaks for MSNPs, observed at 278 cm^{-1} and 376 cm^{-1} correspond to the E_{1g} peak of crystalline MoS_2 and hexagonal morphology of MoS_2, respectively.[28, 32] The peaks observed at 231 cm^{-1} and 330 cm^{-1} are the J_2 and J_3 peaks, corresponding to the existence of a super lattice.[33] Additionally, peaks at 816 cm^{-1} and 987 cm^{-1} correspond to the presence of oxysulfide.[28]

The experimental and control groups used for the mechanical measurements are listed in Table 1. The mechanical properties (compressive modulus, compressive yield strength, flexural modulus and flexural yield strength) of the 2D nanostructure-reinforced crosslinked PPF nanocomposites as a function of 2D nanostructure concentration (0.01–0.2 wt %) are presented in Figure 2 A–D. Also included are the mechanical properties of the crosslinked PPF composite as baseline control, and crosslinked PPF nanocomposites reinforced with 1D carbon nanostructures (SWCNTs and MWCNTs) as positive controls. Table 2 A–D tabulates the highest compressive modulus and yield strength, flexural modulus and yield strength, the corresponding loading concentration for each 2D nanostructure nanocomposite, and % increase compared to the baseline and positive controls.

A significant increase in the compressive modulus (Figure 2A) and yield strength (Figure 2B) was observed for all the 2D nanostructure- nanocomposites at the various loading concentrations compared to PPF composites. Most of the 2D nanostructure nanocomposites, at various loading concentrations, also exhibited significant increases in the compressive modulus, and yield strength compared to 1D nanostructure nanocomposites. The highest compressive modulus values (Table 2A) for the 2D nanostructure nanocomposites were 35–108% greater compared to PPF composites, and up to 78% greater compared to the positive controls. The highest compressive yield strength values (Table 2B) for the 2D nanostructure nanocomposites were 27–93% greater compared to PPF composites, and up to 81% greater compared to the positive controls.

The flexural modulus (Figure 2C) and yield strength (Figure 2D) for all the 2D nanostructure- nanocomposites, at all the loading concentrations, also show a significant increase compared to PPF composites. Additionally, compared to 1D nanostructure nanocomposites, most 2D nanostructure nanocomposites, at various loading concentrations, showed significant increases in the flexural modulus and yield strength. The highest flexural modulus values (Table 2C) for the 2D nanostructure nanocomposites were 15–53% greater compared to PPF composites, and up to 47% greater compared to the 1D nanostructure nanocomposites. The highest flexural yield strength values (Table 2D) for the 2D nanostructure nanocomposites were 102–262% greater compared to PPF composites, and up to 237% greater compared to the positive controls.

The results of the mechanical properties (Figures 2 A–D and Tables 2 A–D) indicate a clear and consistent trend in the values for the 2D nanostructure nanocomposites with MSNP nanocomposites > GONP nanocomposites > MWGONR nanocomposites > SWGONR nanocomposites. The results taken together also indicate that, among the 2D nanostructures, nanoplatelets are better reinforcing agents than nanoribbons, and that inorganic 2D

nanostructures reinforce the PPF polymer significantly better than 2D carbon nanostructures. The range of values of the Young's modulus, compressive strength, flexural modulus and flexural strength for the 2D nanostructure-reinforced PPF nanocomposites are lower than literature values of cortical bone, but greater or comparable to trabecular bone. For load bearing applications, an orthopedic implant should ideally have mechanical properties similar to native bone. Orthopedic implants with lower or higher mechanical properties compared to the native bone could elicit structural failure or stress shielding, respectively. From the above analysis (Table 3) it can inferred PPF nanocomposites can be fabricated with all 2D nanostructures as reinforcing agents towards tissue engineering strategies for trabecular bone.

The significantly higher mechanical properties of the 2D nanostructure-reinforced nanocomposites compared to the baseline or positive controls may be attributed to differences in the dependence or interdependence of three important factors: surface area, aspect ratio, and crosslinking density. Higher surface area of the nanoparticles dispersed in polymer matrix has been shown to permit efficient load transfer from the polymer matrix to the nanoparticles.[34] The measured BET surface areas of all the nanostructures are listed in Table 4. The values follow the following trend: MWGONR > SWCNTs > MWCNTs > SWGONRs > GONPs > MSNPs. Surface area values of SWCNTs, MWCNTs, MWGONRs, GONPs and MSNPs, are within the range reported in the literature.[8, 34–39] The values for SWGONRs have not been reported previously, and are lower than that of SWCNTs. Interestingly; the surface areas of graphene nanoparticles (SWGONRs, MWGONRs, and GONPs) are lower than the theoretical value of 2630 m^2/g for individual isolated graphene sheets. It is important to note that, for the solid nanostructure samples, a significant surface area is not available for nitrogen absorption due the presence of nanoparticles as aggregated bundles.[31, 40] However, during the preparation of polymeric nanocomposites, sonication could disrupt the aggregates, and further increase the surface area of all the nanostructures. There is no method that allows direct quantitative determination of the surface of the nanostructures in the polymer matrix. Nevertheless, the above results suggest that the surface area of nanostructures may not be the major factor responsible for the observed trends in the mechanical properties.

The aspect ratio of fillers has been reported to affect the mechanical properties of polymer composites.[41] Table 5 lists the aspect ratio of the various nanostructures used in this study. The values follow trend: nanoplatelets < nanoribbons < nanotubes; opposite of that observed for the mechanical properties. The trend suggests that decrease in the aspect ratio (an important measure of size) of the 2D nanostructures leads to increase in the mechanical properties of the nanocomposites. However, this relationship between aspect ratio and mechanical properties cannot at least be extrapolated for hydrophilic polymer nanocomposites reinforced with other 2D nanostructures. For instance, a recent study on pristine graphene-reinforced poly(vinyl alcohol) (PVA) polymer nanocomposites shows that its Young's modulus increased with increase in the aspect ratio of pristine graphene sheets.[42]

Sol fraction analysis was performed to assess changes in the crosslinking density of PPF in the presence of 2D nanostructures, since changes in the crosslinking density have been shown to alter the mechanical properties of nanoparticle-reinforced polymer nanocomposites.[43] A decrease in the sol fraction values signifies an increase in the crosslinking density of the polymer.[24] Sol fractions measured for various crosslinked nanocomposites are reported in Figure 4. Sol fraction values for PPF, SWCNT and MWCNT composites was ≈ 14%, ≈ 12.9–14.2% and ≈ 12.1–14.2%, respectively. The sol fraction for 2D nanocomposite groups was between 10.2–12.2% for SWGONR composites, 8.7–11.6% for MWGONR composites, 9.5–12.3% for GONP composites, and 8.5–10% for

MSNP composites. Higher crosslinking density was observed for all loading concentrations of MSNPs. Additionally, higher loading concentrations (0.1–0.2 wt%) of GONPs and MWGONRs also resulted in significant increases in the crosslinking density of nanocomposites. The sol-fraction results suggest a crosslinking density trend of 2D nanostructure nanocomposites > 1D nanostructures nanocomposites > PPF composites. The presence of substantially higher number hydroxyl, carboxyl, and sulfide functional groups on the 2D nanostructures[8, 28] formed during the synthesis of these nanostructures could result in increased chemical interactions (covalent bonds between nanoparticle and PPF leading to formation of crosslinks) between the 2D nanostructures and the surrounding PPF matrix, and thus, a higher crosslinking density. Consequently, the crosslinking density of nanocomposites may be another factor responsible for the observed differences in trends of the mechanical properties.

Transmission electron microscopy (TEM) was performed on the crosslinked nanocomposites to characterize the dispersion of 1D and 2D nanostructures in the PPF matrix (Figure 4). TEM analysis was performed with caution to minimize the effects of local heating and irradiation on the specimens. No solvent dissipation was observed. The analysis of the TEM images indicated that all the nanostructures were coated with a thin layer of PPF, and embedded in the PPF matrix. The analysis indicated that SWCNTs and MWCNTs were present in the nanocomposites as bundles of 2–4 and 2–3 nanotubes, respectively (Figures 4 A and B). SWGONRs were dispersed as bundles of a few (2–5) nanoribbons, and MWGONRs existed as individual nanoribbons (Figures 4 C and D). GONPs and MSNPs also existed as individual nanoplatelets in the PPF matrix (Figures 4 D and E). The existence of MWGONRs, GONPs and MSNPs as individual nanoparticles (observed in TEM analysis, Figure 4) further corroborates the hypothesis that during the preparation of nanocomposites, sonication could effectively disrupt the aggregation of nanostructures, thereby increasing the surface area available for interaction with the polymer.

The above surface area, aspect ratio, sol fraction and TEM analysis results taken together indicates differences in nanostructure architecture (2D vs. 1D nanostructures), as well as number of functional groups, and structural defects for the 2D nanostructures maybe key properties that affect the mechanical properties of 2D nanostructure-reinforced PPF nanocomposites and the reason for the enhanced mechanical properties compared to the controls. The presence of structural defects and functional groups could allow better nanomaterial-polymer physico-chemical interactions such as increased non-covalent interaction of the polymer with the nanomaterial allowing the polymer to wrap efficiently over the nanomaterials, and formation of nanomaterial-polymer chemical bonds, leading to increases in the crosslinking density in the nanocomposites. Additionally, it could allow better dispersion of the 2D nanostructures in the polymer matrix and thus prevent the formation of large nanostructure aggregates which can cause slippage between nanostructures, or act as sources of stress concentrators, or crack initiators under applied loads.[44] Among the 2D nanostructure nanocomposites, based on the consistently higher values in the mechanical properties for nanoplatelets compared to nanoribbons, it can be inferred that, other than differences in crosslinking density, the lower aspect ratio of nanoplatelets compared to nanoribbons may be responsible for their better mechanical reinforcement. Additionally, MSNPs lead to equivalent or better mechanical reinforcement suggesting that chemical composition of the nanostructures may also play a role, and that inorganic 2D nanostructures maybe more suitable to achieve enhancement for certain mechanical properties (e.g. compressive mechanical properties) compared to carbon nanostructures.

To the best of our knowledge, this is the first report investigating, and comparing the efficacy of nanotubes, nanoribbons and nanoplatelets as well as inorganic and carbon

nanomaterials as reinforcing agents towards the fabrication of polymeric nanocomposites as biomedical implants for bone tissue engineering. Previous studies have investigated the efficacy of fullerenes, and SWCNTs as reinforcing agents of crosslinked PPF nanocomposites. In those studies, fullerenes marginally increased the mechanical properties (~10% increase in compressive or flexural modulus) compared to PPF composites. Pristine SWCNT-reinforced PPF nanocomposites showed up to 65% increase in the compressive modulus and 69% increase in the flexural modulus at a loading between 0.02–0.1 wt% of SWCNTs.[5] Functionalization or reduction in the aspect ratio of the SWCNTs further improved (up to 2-fold increase in compressive and flexural modulus) the mechanical properties.[3, 24] No direct comparisons can be made between the results of this study with those results due to differences in crosslinking agent (NVP vs. PPF-diacrylate), crosslinking method (thermal vs. photocrosslinking) and/or curing temperatures (60°C vs. 37°C).[5, 24] Nonetheless, the results of those studies provide two additional strategies that can be employed to further improve the mechanical properties of 2D nanostructure-reinforced PPF nanocomposites: (1) Covalent functionalization of individual 2D nanostructures to further improve their dispersion in the polymer matrix and to prevent the formation of aggregates, and (2) reduction of their aspect ratio (especially for the nanoribbons).

In general for polymeric nanocomposites, few reports have investigated the mechanical properties of 2D carbon or inorganic nanostructures[45–49] compared to carbon nanotubes.[2, 3, 5, 15, 22, 24, 50, 51] Song et al. reported ≈ 74% increase in the Young's modulus of polypropylene composites compared to pristine polymer composite controls at 0.42 vol% loading of exfoliated graphene platelets.[45] Compared to epoxy composite controls, Koratkar, Tour, and coworkers reported ≈ 31% and ≈ 30% increases in the Young's modulus of epoxy composites at ≈ 0.1 wt% loading of graphene platelets[47] and 0.3 wt% loading of MWGONRs,[34] respectively. Pinto et al. reported ≈ 100% increase in the yield strength and Young's modulus of PLGA nanocomposite films (compared to pristine PLGA films) at about 0.4 wt% loading of exfoliated graphene oxide sheets and graphene nanoplatelets.[46] In comparison to pristine thermoplastic polymer- polyamide, Chatterjee et al. reported ≈ 80% improvement in the modulus of toughness at 0.5 wt% loading of surfactant dispersed graphene nanoplatelets.[49] Recently, compared to pristine polyvinyl alcohol (PVA) composites, Zhou et al. reported ≈ 28% increase in the storage modulus and ≈ 24% increase in the tensile strength upon the addition of 1–5 wt% exfoliated molybdenum disulfide nanosheets.[52] The results of these various reports cannot be directly compared due to variations in the polymer matrix, the fabrication method of the polymeric nanocomposites, and the chemical state (pristine or functionalized) of the nanomaterials. However, these other studies corroborate a salient result of this study that the 2D nanostructures can substantially enhance the mechanical properties of polymer nanocomposites even at very low loading concentrations. This work also significantly contributes to existing body of work 2D nanostructure-reinforced polymer nanocomposites by providing direct comparisons of the efficacies of various 2D carbon and inorganic 2D nanostructures as reinforcing agents of polymer nanocomposites. Additionally, the promising mechanical property results of the 2D nanostructures reinforced PPF nanocomposites expand their biomedical application for possible bone tissue engineering applications and opens avenues for *in vitro* and *in vivo* studies to assess their safety and efficacy.

Conclusions

In conclusion, biodegradable polymeric nanocomposites of PPF reinforced with various 2D nanostructures (SWGONRs, MWGONRs, GONPs, MSNPs) at low loading concentrations (were fabricated towards the development of implants with improved mechanical properties for bone tissue engineering applications. The mechanical properties (compressive modulus, compressive yield strength, flexural modulus and flexural yield strength) of all the 2D

nanostructure-reinforced crosslinked PPF nanocomposites as a function of 2D nanostructure concentration (0.01–0.2 wt %) were significantly higher in comparison to PPF composites. Most of the 2D nanostructure nanocomposites, at various loading concentrations, also exhibited significant increases compared to 1D nanostructure (pristine SWCNTs and MWCNTs) nanocomposites. The extent of mechanical reinforcement is closely dependent on the nanostructure morphology and follows the trend nanoplatelets > nanoribbons > nanotubes. The inorganic 2D nanostructure MSNPs consistently showed better mechanical reinforcement than 1D or 2D carbon nanostructures. The 2D nanostructures increase the crosslinking density of PPF nanocomposites compared to 1D nanostructures nanocomposites or PPF composites. All the 2D nanostructures except SWGONRs were present as individual particles in the PPF matrix, while SWGONRs, SWCNTs and MWCNTs were present in the PPF matrix as small aggregates (bundles of 2–5 nanoparticles). The study demonstrates that harnessing the reinforcing potential of 2D nanostructures could lead to whole new classes of ultra-strong, lightweight biomaterials for tissue engineering applications.

Acknowledgments

This work was supported by the National Institutes of Health (grants No. 1DP2OD007394-01).

References

1. Dinopoulos H, Dimitriou R, Giannoudis PV. Bone graft substitutes: What are the options? Surgeon. 2012; 10(4):230–9. [PubMed: 22682580]
2. Sitharaman B, Shi X, Walboomers XF, Liao H, Cuijpers V, Wilson LJ, Mikos AG, Jansen JA. In vivo biocompatibility of ultra-short single-walled carbon nanotube/biodegradable polymer nanocomposites for bone tissue engineering. Bone. 2008; 43(2):362–70. [PubMed: 18541467]
3. Sitharaman B, Shi X, Tran LA, Spicer PP, Rusakova I, Wilson LJ, Mikos AG. Injectable in situ cross-linkable nanocomposites of biodegradable polymers and carbon nanostructures for bone tissue engineering. J Biomater Sci Polym Ed. 2007; 18(6):655–71. [PubMed: 17623549]
4. Mistry AS, Pham QP, Schouten C, Yeh T, Christenson EM, Mikos AG, Jansen JA. In vivo bone biocompatibility and degradation of porous fumarate-based polymer/alumoxane nanocomposites for bone tissue engineering. J Biomed Mater Res A. 2010; 92(2):451–62. [PubMed: 19191316]
5. Shi X, Hudson JL, Spicer PP, Tour JM, Krishnamoorti R, Mikos AG. Rheological behaviour and mechanical characterization of injectable poly(propylene fumarate)/single-walled carbon nanotube composites for bone tissue engineering. Nanotechnology. 2005; 16(7):S531–8. [PubMed: 21727474]
6. Cheng Q, Rutledge K, Jabbarzadeh E. Carbon Nanotube-Poly(lactide-co-glycolide) Composite Scaffolds for Bone Tissue Engineering Applications. Ann Biomed Eng. 2013 (Epub ahead of print). 10.1007/s10439-012-0728-8
7. Stankovich S, Dikin DA, Dommett GHB, Kohlhaas KM, Zimney EJ, Stach EA, Piner RD, Nguyen ST, Ruoff RS. Graphene-based composite materials. Nature. 2006; 442(7100):282–286. [PubMed: 16855586]
8. Kosynkin DV, Higginbotham AL, Sinitskii A, Lomeda JR, Dimiev A, Price BK, Tour JM. Longitudinal unzipping of carbon nanotubes to form graphene nanoribbons. Nature. 2009; 458(7240):872–6. [PubMed: 19370030]
9. Dallavalle M, Sandig N, Zerbetto F. Stability, dynamics, and lubrication of MoS2 platelets and nanotubes. Langmuir. 2012; 28(19):7393–400. [PubMed: 22530739]
10. Radisavljevic B, Radenovic A, Brivio J, Giacometti V, Kis A. Single-layer MoS2 transistors. Nat Nanotechnol. 2011; 6(3):147–50. [PubMed: 21278752]
11. Nair RR, Wu HA, Jayaram PN, Grigorieva IV, Geim AK. Unimpeded permeation of water through helium-leak-tight graphene-based membranes. Science. 2012; 335(6067):442–4. [PubMed: 22282806]
12. Zhang Y, Nayak TR, Hong H, Cai W. Graphene: a versatile nanoplatform for biomedical applications. Nanoscale. 2012; 4(13):3833–42. [PubMed: 22653227]

13. Kim JE, Han TH, Lee SH, Kim JY, Ahn CW, Yun JM, Kim SO. Graphene Oxide Liquid Crystals. Angewandte Chemie International Edition. 2011; 50(13):3043–3047.
14. Lalwani G, Kwaczala AT, Kanakia S, Patel SC, Judex S, Sitharaman B. Fabrication and characterization of three-dimensional macroscopic all-carbon scaffolds. Carbon. 2013; 53(0):90–100. [PubMed: 23436939]
15. Shi X, Sitharaman B, Pham QP, Liang F, Wu K, Edward Billups W, Wilson LJ, Mikos AG. Fabrication of porous ultra-short single-walled carbon nanotube nanocomposite scaffolds for bone tissue engineering. Biomaterials. 2007; 28(28):4078–90. [PubMed: 17576009]
16. Shen J, Zhu Y, Yang X, Li C. Graphene quantum dots: emergent nanolights for bioimaging, sensors, catalysis and photovoltaic devices. Chemical Communications. 2012; 48(31):3686–3699. [PubMed: 22410424]
17. Mullick Chowdhury S, Lalwani G, Zhang K, Yang JY, Neville K, Sitharaman B. Cell specific cytotoxicity and uptake of graphene nanoribbons. Biomaterials. 2013; 34(1):283–93. [PubMed: 23072942]
18. Lee C, Wei X, Kysar JW, Hone J. Measurement of the elastic properties and intrinsic strength of monolayer graphene. Science. 2008; 321(5887):385–8. [PubMed: 18635798]
19. Castellanos-Gomez A, Poot M, Steele GA, van der Zant HSJ, Agraït N, Rubio-Bollinger G. Elastic Properties of Freely Suspended MoS2 Nanosheets. Advanced Materials. 2012; 24(6):772–775. [PubMed: 22231284]
20. Bertolazzi S, Brivio J, Kis A. Stretching and breaking of ultrathin MoS2. ACS Nano. 2011; 5(12): 9703–9. [PubMed: 22087740]
21. Yu MF, Lourie O, Dyer MJ, Moloni K, Kelly TF, Ruoff RS. Strength and Breaking Mechanism of Multiwalled Carbon Nanotubes Under Tensile Load. Science. 2000; 287(5453):637–640. [PubMed: 10649994]
22. Ajayan PM, Tour JM. Materials Science: Nanotube composites. Nature. 2007; 447(7148):1066–1068. [PubMed: 17597753]
23. Mistry AS, Mikos AG. Tissue engineering strategies for bone regeneration. Adv Biochem Eng Biotechnol. 2005; 94:1–22. [PubMed: 15915866]
24. Shi X, Hudson JL, Spicer PP, Tour JM, Krishnamoorti R, Mikos AG. Injectable nanocomposites of single-walled carbon nanotubes and biodegradable polymers for bone tissue engineering. Biomacromolecules. 2006; 7(7):2237–42. [PubMed: 16827593]
25. Yaszemski MJ, Payne RG, Hayes WC, Langer RS, Aufdemorte TB, Mikos AG. The ingrowth of new bone tissue and initial mechanical properties of a degrading polymeric composite scaffold. Tissue Eng. 1995; 1(1):41–52. [PubMed: 19877914]
26. Kasper FK, Tanahashi K, Fisher JP, Mikos AG. Synthesis of poly(propylene fumarate). Nat Protoc. 2009; 4(4):518–25. [PubMed: 19325548]
27. Paratala BS, Jacobson BD, Kanakia S, Francis LD, Sitharaman B. Physicochemical characterization, and relaxometry studies of micro-graphite oxide, graphene nanoplatelets, and nanoribbons. PLoS One. 2012; 7(6):e38185. [PubMed: 22685555]
28. Castro-Guerrero CF, Deepak FL, Ponce A, Cruz-Reyes J, Valle-Granados MD, Fuentes-Moyado S, Galvan DH, Jose-Yacaman M. Structure and catalytic properties of hexagonal molybdenum disulfide nanoplates. Catalysis Science & Technology. 2011; 1(6):1024–1031.
29. Stankovich S, Dikin DA, Piner RD, Kohlhaas KA, Kleinhammes A, Jia Y, Wu Y, Nguyen ST, Ruoff RS. Synthesis of graphene-based nanosheets via chemical reduction of exfoliated graphite oxide. Carbon. 2007; 45(7):1558–1565.
30. Stankovich S, Piner RD, Nguyen ST, Ruoff RS. Synthesis and exfoliation of isocyanate-treated graphene oxide nanoplatelets. Carbon. 2006; 44(15):3342–3347.
31. Srinivas G, Zhu Y, Piner R, Skipper N, Ellerby M, Ruoff R. Synthesis of graphene-like nanosheets and their hydrogen adsorption capacity. Carbon. 2010; 48(3):630–635.
32. Wieting TJ, Verble JL. Infrared and Raman Studies of Long-Wavelength Optical Phonons in Hexagonal MoS_{2}. Physical Review B. 1971; 3(12):4286–4292.
33. Yang D, Sandoval SJ, Divigalpitiya WMR, Irwin JC, Frindt RF. Structure of single-molecular-layer MoS_{2}. Physical Review B. 1991; 43(14):12053–12056.

34. Rafiee MA, Lu W, Thomas AV, Zandiatashbar A, Rafiee J, Tour JM, Koratkar NA. Graphene nanoribbon composites. ACS Nano. 2010; 4(12):7415–20. [PubMed: 21080652]
35. Girishkumar G, Hall TD, Vinodgopal K, Kamat PV. Single wall carbon nanotube supports for portable direct methanol fuel cells. J Phys Chem B. 2006; 110(1):107–14. [PubMed: 16471506]
36. Agnihotri S, Mota JP, Rostam-Abadi M, Rood MJ. Structural characterization of single-walled carbon nanotube bundles by experiment and molecular simulation. Langmuir. 2005; 21(3):896–904. [PubMed: 15667165]
37. Ajayan PM. Nanotubes from Carbon. Chemical Reviews. 1999; 99(7):1787–1800. [PubMed: 11849010]
38. Lehman JH, Terrones M, Mansfield E, Hurst KE, Meunier V. Evaluating the characteristics of multiwall carbon nanotubes. Carbon. 2011; 49(8):2581–2602.
39. Elizondo-Villarreal N, Velázquez-Castillo R, Galván DH, Camacho A, José Yacamán M. Structure and catalytic properties of molybdenum sulfide nanoplatelets. Applied Catalysis A: General. 2007; 328(1):88–97.
40. Kim WS, Kim YI, Kim HJ, Hwanag JY, Moon SY, Park NH, Shim KB, Kim HW, Ham H, Huh H. Fabrication of a large scale transparent conducting film using transformed few-layered graphene nanoribbons obtained from unzipping of single wall carbon nanotubes. Journal of Materials Chemistry. 2011; 21(39):15655–15659.
41. Kardos JL. Critical issues in achieving desirable mechanical properties for short fiber composites. Pure Appl Chem. 1985; 57(11):1651–1657.
42. May P, Khan U, O'Neill A, Coleman JN. Approaching the theoretical limit for reinforcing polymers with graphene. Journal of Materials Chemistry. 2012; 22(4):1278–1282.
43. Fisher JP, Dean D, Mikos AG. Photocrosslinking characteristics and mechanical properties of diethyl fumarate/poly(propylene fumarate) biomaterials. Biomaterials. 2002; 23(22):4333–43. [PubMed: 12219823]
44. Ajayan PM, Banhart F. Strong bundles. Nat Mater. 2004; 3(3):135–6. [PubMed: 14991009]
45. Song P, Cao Z, Cai Y, Zhao L, Fang Z, Fu S. Fabrication of exfoliated graphene-based polypropylene nanocomposites with enhanced mechanical and thermal properties. Polymer. 2011; 52(18):4001–4010.
46. Pinto AM, Cabral J, Tanaka DAP, Mendes AM, Magalhães FD. Effect of incorporation of graphene oxide and graphene nanoplatelets on mechanical and gas permeability properties of poly(lactic acid) films. Polymer International. 2013; 62(1):33–40.
47. Rafiee MA, Rafiee J, Wang Z, Song H, Yu ZZ, Koratkar N. Enhanced mechanical properties of nanocomposites at low graphene content. ACS Nano. 2009; 3(12):3884–90. [PubMed: 19957928]
48. Wang Y, Shi Z, Yin J. Unzipped Multiwalled Carbon Nanotubes for Mechanical Reinforcement of Polymer Composites. The Journal of Physical Chemistry C. 2010; 114(46):19621–19628.
49. Chatterjee S, Nüesch FA, Chu BTT. Comparing carbon nanotubes and graphene nanoplatelets as reinforcements in polyamide 12 composites. Nanotechnology. 2011; 22(27):275714. [PubMed: 21613677]
50. Coleman JN, Khan U, Blau WJ, Gun'ko YK. Small but strong: A review of the mechanical properties of carbon nanotube–polymer composites. Carbon. 2006; 44(9):1624–1652.
51. Lin C, Wang Y, Lai Y, Yang W, Jiao F, Zhang H, Ye S, Zhang Q. Incorporation of carboxylation multiwalled carbon nanotubes into biodegradable poly(lactic-co-glycolic acid) for bone tissue engineering. Colloids Surf B Biointerfaces. 2011; 83(2):367–75. [PubMed: 21208787]
52. Zhou K, Jiang S, Bao C, Song L, Wang B, Tang G, Hu Y, Gui Z. Preparation of poly(vinyl alcohol) nanocomposites with molybdenum disulfide (MoS2): structural characteristics and markedly enhanced properties. RSC Advances. 2012; 2(31):11695–11703.
53. Rho JY, Ashman RB, Turner CH. Young's modulus of trabecular and cortical bone material: ultrasonic and microtensile measurements. J Biomech. 1993; 26(2):111–9. [PubMed: 8429054]
54. Schoenfeld C, Lautenschlager E, Meyer P. Mechanical properties of human cancellous bone in the femoral head. Medical and Biological Engineering and Computing. 1974; 12(3):313–317.
55. O'Kelly K, Tancred D, McCormack B, Carr A. A quantitative technique for comparing synthetic porous hydroxyapatite structures and cancellous bone. Journal of Materials Science: Materials in Medicine. 1996; 7(4):207–213.

56. Choi K, Kuhn JL, Ciarelli MJ, Goldstein SA. The elastic moduli of human subchondral, trabecular, and cortical bone tissue and the size-dependency of cortical bone modulus. J Biomech. 1990; 23(11):1103–13. [PubMed: 2277045]

57. Du C, Ma H, Ruo M, Zhang Z, Yu X, Zeng Y. An experimental study on the biomechanical properties of the cancellous bones of distal femur. Bio-medical materials and engineering. 2006; 16(3):215–222. [PubMed: 16518020]

58. REILLY DT, BURSTEIN AH. The mechanical properties of cortical bone. The Journal of Bone and Joint Surgery (American). 1974; 56(5):1001–1022.

59. SUCHÝ T, BALÍK K, ČERNÝ M, SOCHOR M, HULEJOVÁ H, PEŠÁKOVÁ V, FENCLOVÁ T. A composite based on glass fibers and siloxane matrix as a bone replacement. Ceramics-Silikáty. 2008; 52(1):29–36.

60. Cinke M, Li J, Chen B, Cassell A, Delzeit L, Han J, Meyyappan M. Pore structure of raw and purified HiPco single-walled carbon nanotubes. Chemical Physics Letters. 2002; 365(1–2):69–74.

61. Jeon IY, Shin YR, Sohn GJ, Choi HJ, Bae SY, Mahmood J, Jung SM, Seo JM, Kim MJ, Wook Chang D, Dai L, Baek JB. Edge-carboxylated graphene nanosheets via ball milling. Proc Natl Acad Sci U S A. 2012; 109(15):5588–93. [PubMed: 22454492]

Figure 1 A:

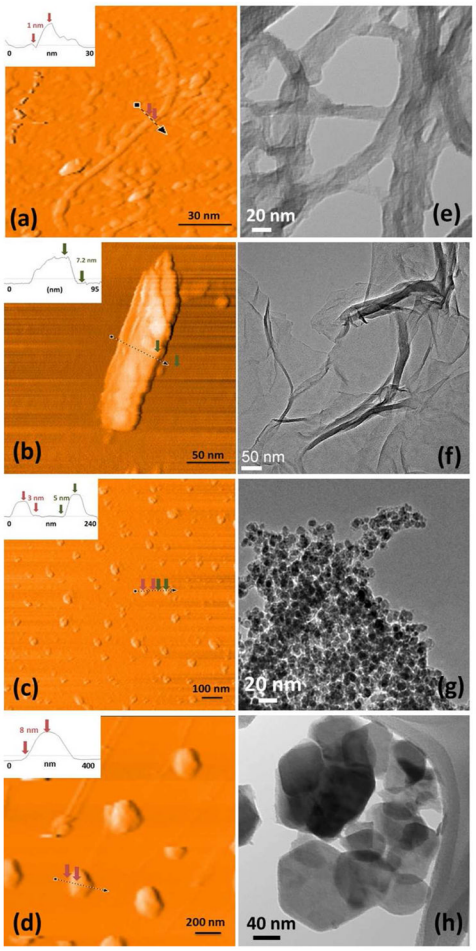

Figure 1 B:

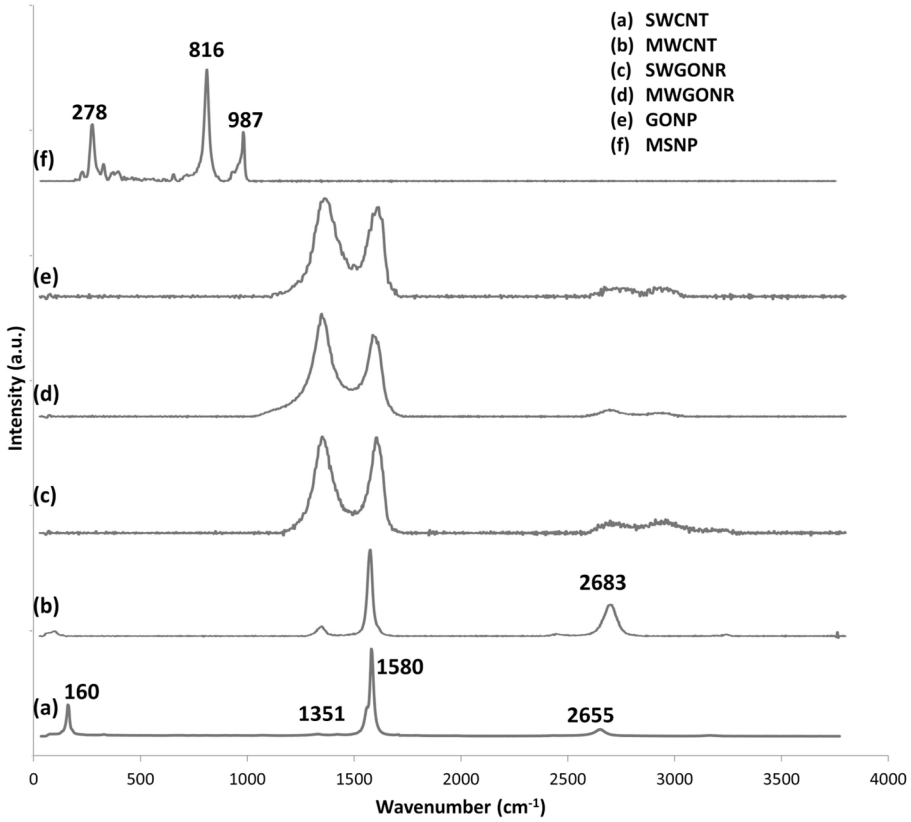

Figure 1.

(A) AFM (a–d) and TEM (e–f) images of SWGONR, MWGONR, GONP and MSNP, respectively. Inset in a–d are height profiles (Z) of nanostructures. (B) Representative Raman spectra of (a) SWCNT, (b) MWCNT, (c) SWGONR, (d) MWGONR, (e) GONP, and (f) MSNP, respectively.

Figure 2A

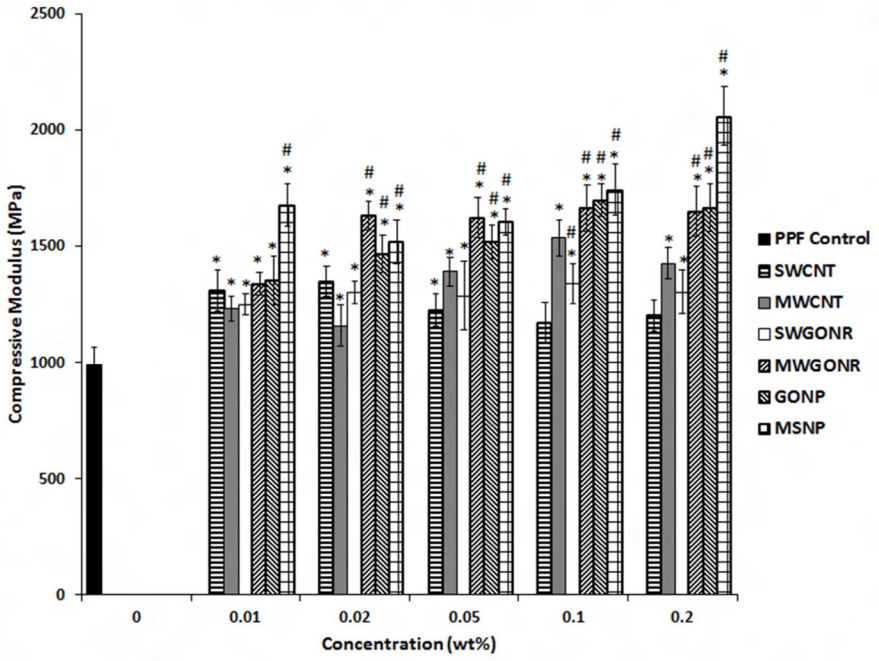

Figure 2B

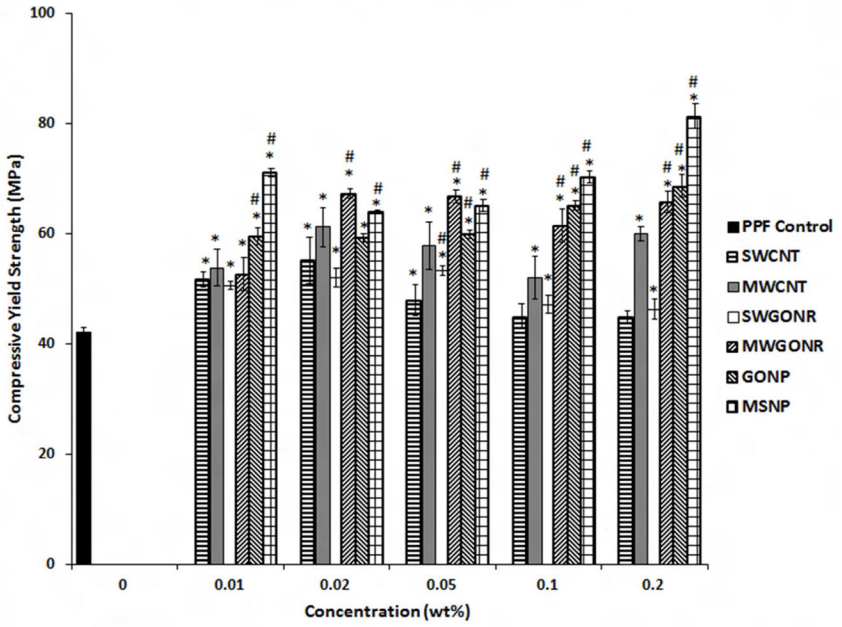

Figure 2C

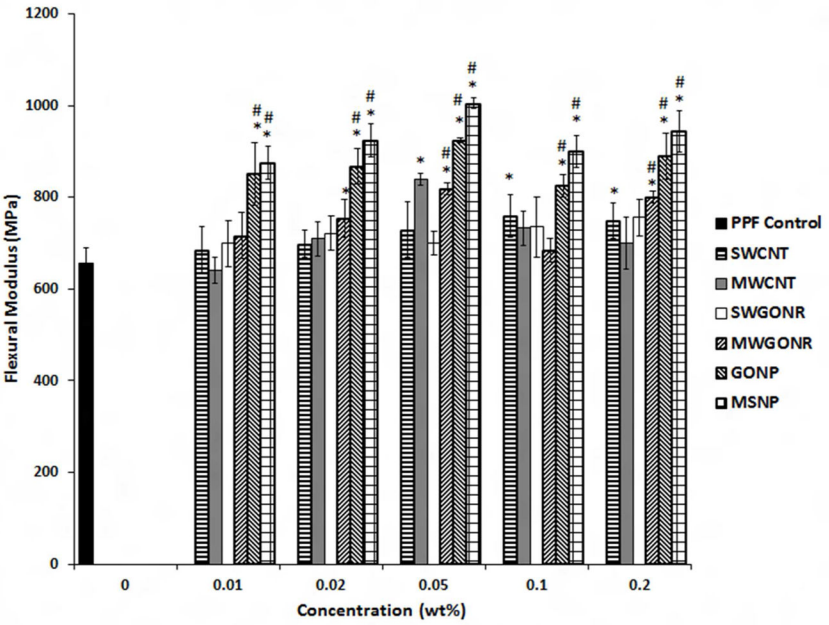

Figure 2D

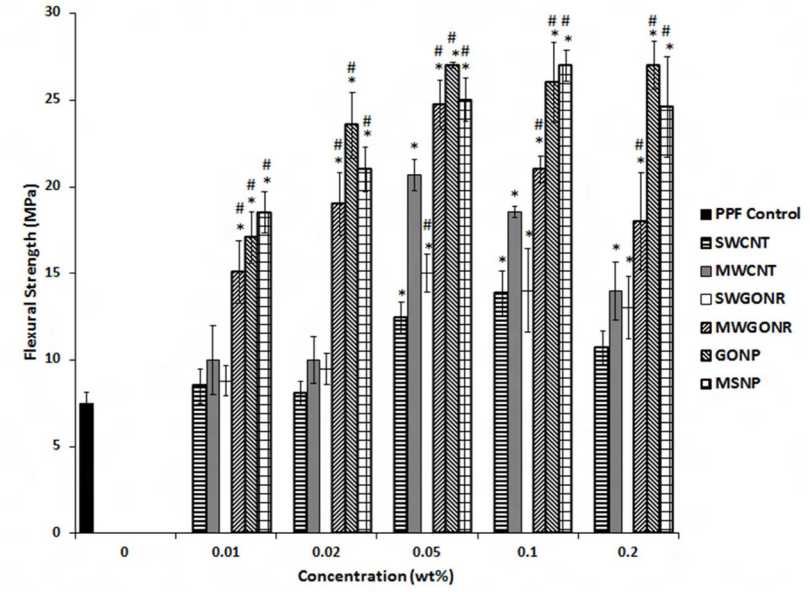

Figure 2.

(A) compressive modulus, (B) compressive yield strength, (C) flexural modulus and (D) flexural yield strength of PPF nanocomposites as a function of nanostructure loading concentration. Error bars represent mean ± standard deviation for n=5. Groups with a significant difference compared to PPF composite are marked with the symbol "*" and with a significant difference compared to positive controls (either SWCNT composites, or MWCNT composites, or both SWCNT and MWCNT composites) are marked with "#" ($p < 0.05$).

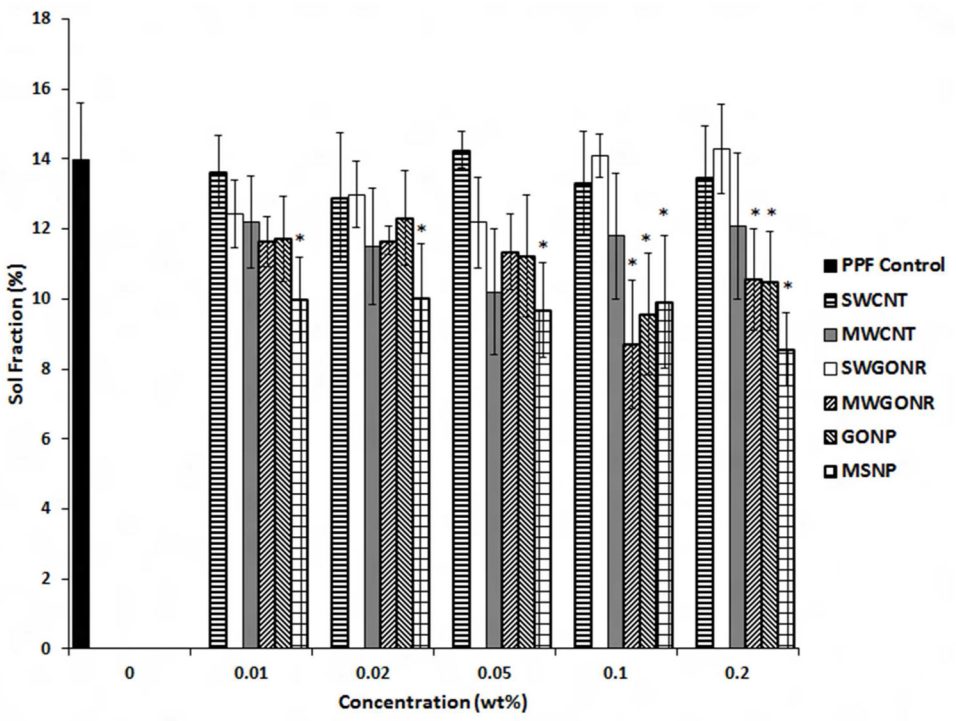

Figure 3.
Sol fraction analysis of crosslinked PPF nanocomposites as a function of nanostructure loading (mean ± standard deviation for n=5 samples). Groups with a significant difference compared to PPF composite are marked with the symbol "*" ($p < 0.05$).

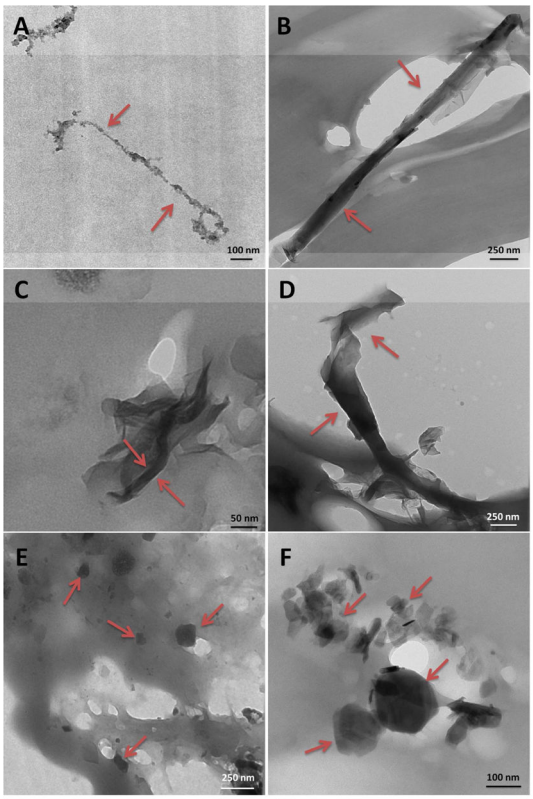

Figure 4.
Representative transmission electron microscopy images of crosslinked PPF nanocomposites at 0.1 wt% loading of (A) SWCNT, (B) MWCNT, (C) SWGONR, (D) MWGONR, (E) GONP and (F) MSNP. Nanostructures are marked with red arrows.

Table 1

Experimental and control groups used for mechanical testing

Name	Abbreviation
PPF	Polypropylene fumarate
SWCNT	Single walled carbon nanotubes
MWCNT	Multi walled carbon nanotubes
SWGONR	Single walled graphene oxide nanoribbons
MWGONR	Multi walled graphene oxide nanoribbons
GONP	Graphene oxide nanoplatelets
MSNP	Molybdenum disulfide nanoplatelets

Table 2A

Compressive modulus of various 2D nanostructure reinforced PPF nanocomposites

2D Nanostructure	Highest compressive modulus (MPa)	Concentration (wt %)	% increase compared to PPF	% increase compared to SWCNTs	% increase compared to MWCNTs
SWGONR	1340.4 ± 83.6	0.1	35.3	0–12.4	0–15.7
MWGONR	1665.2 ± 99.0	0.1	68.1	23.3–41.9	8.3–43.7
GONP	1699.3 ± 69.4	0.1	71.6	25.8–44.7	10.6–46.7
MSNP	2061.8 ± 126.6	0.2	108.1	52.6–75.5	34.1–77.9

Table 2B

Compressive yield strength of various 2D nanostructure reinforced PPF nanocomposites

2D Nanostructure	Highest compressive yield strength (MPa)	Concentration (wt %)	% increase compared to PPF	% increase compared to SWCNTs	% increase compared to MWCNTs
SWGONR	53.2 ± 0.8	0.05	26.5	0–18.7	0–2.3
MWGONR	67.4 ± 1.1	0.02	60.1	22.1–50.3	10–29.5
GONP	68.6 ± 2.0	0.2	63.1	24.3–53.1	12–32
MSNP	81.3 ± 2.2	0.2	93.2	47.3–81.4	32.7–56.4

Table 2C

Flexural modulus of various 2D nanostructure reinforced PPF nanocomposites

2D Nanostructure	Highest flexural modulus (MPa)	Concentration (wt %)	% increase compared to PPF	% increase compared to SWCNTs	% increase compared to MWCNTs
SWGONR	756.3 ± 40.2	0.2	15.0	0–10.3	0–17.9
MWGONR	817.6 ± 12.6	0.05	24.4	7.6–19.2	0–27.5
GONP	925.2 ± 5.4	0.05	40.7	21.7–34.9	10.2–44.2
MSNP	1005.8 ± 12.3	0.05	53.0	32.2–46.6	19.7–56.7

Table 2D

Flexural yield strength of various 2D nanostructure reinforced PPF nanocomposites

2D Nanostructure	Highest flexural yield strength (MPa)	Concentration (wt %)	% increase compared to PPF	% increase compared to SWCNTs	% increase compared to MWCNTs
SWGONR	15.1 ± 0.8	0.05	101.7	9.3–87	0–51.5
MWGONR	24.7 ± 1.4	0.05	230.1	78.9–206.1	19.5–148.0
GONP	27.2 ± 0.1	0.05	263.1	96.8–236.7	31.5–172.8
MSNP	27.1 ± 0.9	0.1	262.2	96.3–235.8	31.1–172.1

Table 3

Mechanical properties of human cortical and trabecular bone with various 2D nanostructure reinforced PPF nanocomposites

Mechanical Properties	Young's modulus (GPa)	Compressive yield strength (MPa)	Flexural modulus (GPa)	Flexural yield strength (MPa)
Trabecular bone[53–57]	0.3–10	0.1–13	0.04–0.05	1.8–10
Cortical bone[53, 56, 58, 59]	12–20	170–193	5–23	133–295
SWGONR	1.2–1.3	46.3–53.2	0.7–0.75	8.8–15.1
MWGONR	1.3–1.6	52.6–67.4	0.68–0.81	15.1–24.7
GONP	1.3–1.7	59.2–68.6	0.82–0.92	17–27.2
MSNP	1.5–2	64–81.3	0.87–1.0	18.5–27.1

Table 4

BET surface area of various nanostructures

Nanostructure	Surface area (m^2/g)	
	Measured	**Reported**
SWCNT	353.8	81–1587 [35, 36, 60]
MWCNT	211.5	20–1315 [37, 38]
SWGONR	96.3	Not available
MWGONR	384.4	436–511 [8, 34]
GONP	44.6	29–466 [29, 61]
MSNP	16.7	8–60 [39]

Table 5

Average aspect ratios of various nanostructures

Nanostructure	Aspect ratio*
	Measured
SWCNT	> 1000
MWCNT	> 1000
SWGONR	≈ 80–350
MWGONR	≈ 5–25
GONP	≈ 1
MSNP	≈ 1

*Aspect ratio = (length along long axis/length along short axis)